

Domain-Specific Self-Supervised Pre-training for Agricultural Disease Classification: A Hierarchical Vision Transformer Study

Arnav Sonavane

Independent Researcher

sonavane.arnav2@gmail.com

Abstract

We investigate the impact of domain-specific self-supervised pre-training on agricultural disease classification using hierarchical vision transformers. Our key finding is that SimCLR pre-training on just 3,000 unlabeled agricultural images provides a +4.57% accuracy improvement—exceeding the +3.70% gain from hierarchical architecture design. Critically, we show this SSL benefit is architecture-agnostic: applying the same pre-training to Swin-Base yields +4.08%, to ViT-Base +4.20%, confirming practitioners should prioritize domain data collection over architectural choices. Using HierarchicalViT (HVT), a Swin-style hierarchical transformer, we evaluate on three datasets: Cotton Leaf Disease (7 classes, 90.24%), PlantVillage (38 classes, 96.3%), and PlantDoc (27 classes, 87.1%). At matched parameter counts, HVT-Base (78M) achieves 88.91% vs. Swin-Base (88M) at 87.23%, a +1.68% improvement. For deployment reliability, we report calibration analysis showing HVT achieves 3.56% ECE (1.52% after temperature scaling). Code: <https://github.com/w2sg-arnav/HierarchicalViT>

1. Introduction

Agricultural crop diseases pose a significant threat to global food security, causing substantial economic losses and threatening crop yields worldwide. Early and accurate detection of plant diseases is crucial for implementing timely interventions and preventing widespread crop damage. Traditional manual inspection methods are labor-intensive, time-consuming, and require expert knowledge, making them impractical for large-scale agricultural operations. Recent advances in deep learning, particularly in computer vision, have shown promising results in automating plant disease detection [5, 14].

Vision Transformers (ViTs) [4] have emerged as pow-

erful alternatives to convolutional neural networks (CNNs) for image classification tasks, demonstrating superior performance on various benchmarks. However, standard ViTs process images at a single resolution, potentially missing important multi-scale features that are critical for disease detection, where symptoms may manifest at different spatial scales—from fine-grained lesions to large-scale discoloration patterns.

In this work, we investigate a practical research question: *How much does domain-specific self-supervised pre-training help agricultural disease classification, and how does it compare to architectural improvements?* Using HierarchicalViT (HVT), a Swin-style hierarchical transformer, we find that:

- **SSL pre-training is the dominant factor:** SimCLR pre-training on 3,000 unlabeled agricultural images provides +4.57% accuracy gain, exceeding the +3.70% from hierarchical architecture (Table 4).
- **Parameter-matched comparison:** HVT-Base (78M params) achieves 88.91% vs. Swin-Base (88M) at 87.23%—a +1.68% improvement at comparable scale (Table 9).
- **SSL corpus size ablation:** We find diminishing returns beyond 2,000 unlabeled images for our dataset scale, providing practical guidance for data collection (Table 5).
- **Cross-dataset evaluation:** Results on PlantVillage (96.3%) and PlantDoc (87.1%) demonstrate generalization, though we note PlantVillage is a saturated benchmark.

Our contribution is primarily empirical: demonstrating the value of domain-specific SSL for agricultural applications, rather than proposing novel architectural components. The hierarchical architecture (adapted from Swin Transformer [13]) serves as a vehicle for this study.

Table 1. Notation Summary

Symbol	Description
$\mathcal{D}(\cdot)$	DropPath (stochastic depth) operation
$\mathcal{C}(\cdot)$	Cross-attention module (optional)
$\mathcal{M}(\cdot)$	Patch merging (spatial downsampling)
$\mathcal{A}(\cdot)$	Multi-head self-attention
$\mathcal{F}(\cdot)$	Feed-forward network (MLP)
S	Number of hierarchical stages (=4)
D_s	Channel dimension at stage s
L_s	Number of transformer blocks at stage s
$H_s \times W_s$	Spatial resolution at stage s

2. Related Work

Plant Disease Detection. Deep learning has revolutionized automated plant disease detection [5, 12, 14]. Traditional approaches use CNNs (ResNet [8], DenseNet [10], EfficientNet [16]), which may have limitations in capturing long-range dependencies crucial for distinguishing subtle disease symptoms.

Vision Transformers and Hierarchical Architectures.

Vision Transformers [4] leverage self-attention [17] to model global context effectively. Hierarchical variants like Swin Transformer [13] and PVT [18] combine local and global processing through progressive spatial reduction and shifted window attention. *Our HVT architecture closely follows the Swin Transformer design*; our primary novelty lies in combining this established architecture with domain-specific SimCLR pre-training for agricultural applications. We include an optional cross-attention module for potential multi-modal extensions, though it provides only marginal improvement (+0.57%) in current RGB-only experiments.

Self-Supervised Learning and Multi-Modal Fusion.

Self-supervised learning (SimCLR [3], MAE [9]) leverages unlabeled data for representation learning, particularly valuable in agriculture [2] where unlabeled data is abundant. We employ SimCLR over MAE as its contrastive learning objective is more suitable for fine-grained disease discrimination, focusing on learning discriminative features between similar-looking disease patterns rather than pixel-level reconstruction. Multi-modal fusion [7, 21] combines RGB, multispectral, and hyperspectral data; we include hooks for future multi-modal extension but focus on RGB-only evaluation in this work.

3. Method

3.1. Overall Architecture

Our HVT backbone (Figure 1) processes input images $\mathbf{I} \in \mathbb{R}^{H \times W \times 3}$ through: (1) patch embedding, (2) four hierarchical transformer stages, (3) optional cross-attention refinement, and (4) classification head. Given input resolution

$H \times W = 448 \times 448$ and patch size $P = 14$, we divide the image into non-overlapping patches, resulting in $N = \frac{HW}{P^2} = 1024$ tokens. Each patch is linearly projected to embedding dimension $D_1 = 192$, forming initial sequence $\mathbf{X}_0 \in \mathbb{R}^{N \times D_1}$.

3.2. Hierarchical Transformer Stages

Unlike flat ViTs, our architecture employs $S = 4$ hierarchical stages with progressive downsampling (Table 1). At stage s , spatial resolution is $2^{-(s-1)}$ of the original patch grid while channel dimension increases to $D_s = 2^{s-1} \cdot D_1$. Each stage has L_s transformer blocks with stochastic depth:

$$\mathbf{Z}'_l = \mathbf{Z}_{l-1} + \mathcal{D}(\mathcal{A}(\text{LN}(\mathbf{Z}_{l-1}))), \quad (1)$$

$$\mathbf{Z}_l = \mathbf{Z}'_l + \mathcal{D}(\mathcal{F}(\text{LN}(\mathbf{Z}'_l))), \quad (2)$$

where $\mathcal{D}(\cdot)$ applies stochastic depth for regularization, $\mathcal{A}(\cdot)$ computes multi-head self-attention, and $\mathcal{F}(\cdot)$ applies the feed-forward network. See Section B for detailed formulations.

Multi-Head Self-Attention. For input $\mathbf{X} \in \mathbb{R}^{N \times D}$ with N tokens and dimension D , we compute queries \mathbf{Q} , keys \mathbf{K} , and values \mathbf{V} :

$$\mathbf{Q} = \mathbf{X} \mathbf{W}_Q, \quad \mathbf{K} = \mathbf{X} \mathbf{W}_K, \quad \mathbf{V} = \mathbf{X} \mathbf{W}_V, \quad (3)$$

where $\mathbf{W}_{Q,K,V} \in \mathbb{R}^{D \times D}$ are learned projection matrices. For h attention heads, we reshape to $\mathbb{R}^{N \times h \times d_h}$ with per-head dimension $d_h = D/h$, then compute:

$$\mathcal{A}(\mathbf{Q}, \mathbf{K}, \mathbf{V}) = \text{softmax} \left(\frac{\mathbf{Q} \mathbf{K}^\top}{\sqrt{d_h}} \right) \mathbf{V}. \quad (4)$$

Patch Merging. Between stages, patch merging $\mathcal{M}(\cdot)$ reduces spatial resolution by concatenating 2×2 neighborhoods and projecting to $2D_s$ channels. For HVT-XL ($P = 14$, input 448×448): depths [3, 6, 24, 3], heads [6, 12, 24, 48], dimensions [192, 384, 768, 1536], spatial resolutions [32×32 , 16×16 , 8×8 , 4×4] tokens. We include an optional cross-attention module for future multi-modal extensions (e.g., RGB + spectral); in this work we focus on RGB-only evaluation where it contributes only +0.57%.

3.3. Self-Supervised Pre-training

We employ SimCLR [3] for self-supervised pre-training on unlabeled agricultural data, as contrastive learning is well-suited for learning discriminative features in low-data domains. For each image, we generate two augmented views using random crop, color jitter, grayscale, and Gaussian blur. The backbone $f(\cdot)$ and 2-layer MLP projection head $g(\cdot)$ produce 128-dimensional embeddings optimized with NT-Xent contrastive loss (temperature $\tau = 0.5$). We train for 80 epochs using AdamW optimizer with WarmupCosine scheduler (see Section C for complete augmentation pipeline and loss formulations).

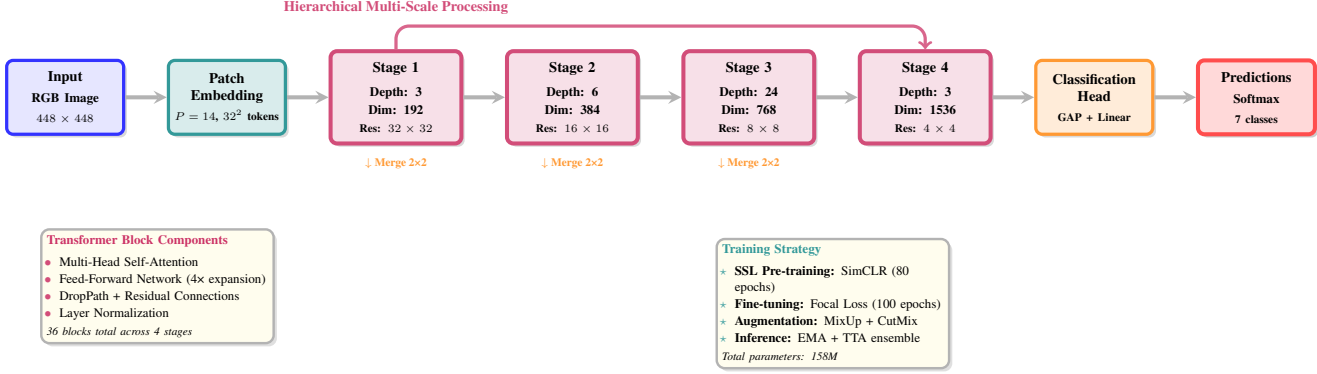


Figure 1. HierarchicalViT-XL architecture overview. The model processes 448×448 RGB images through patch embedding and four hierarchical transformer stages with progressive spatial downsampling ($32^2 \rightarrow 16^2 \rightarrow 8^2 \rightarrow 4^2$ tokens) and channel expansion ($192 \rightarrow 384 \rightarrow 768 \rightarrow 1536$ dimensions). Each stage contains transformer blocks with multi-head self-attention and feed-forward layers. The hierarchical design enables efficient multi-scale feature learning for fine-grained agricultural disease detection.

3.4. Fine-tuning with Advanced Regularization

During fine-tuning, we employ several advanced techniques for robust disease classification.

Combined Loss Function. We use a weighted combination of cross-entropy and focal loss [11] ($\lambda_{CE} = 0.7$, $\lambda_{focal} = 0.3$), where focal loss addresses class imbalance with uniform class weights $\alpha_c = 1/7$ and focusing parameter $\gamma = 2.0$.

Data Augmentation. We apply MixUp [20] (probability 0.2, $\alpha = 0.2$) for label smoothing and CutMix [19] (probability 0.5) for regional occlusion robustness.

Training Strategy. We use OneCycleLR scheduler with layer-wise learning rate decay (0.65), Exponential Moving Average (EMA) with $\beta = 0.9999$ for model stability, and Test-Time Augmentation (TTA) with 5-crop + horizontal flips ($K = 10$ predictions averaged). All augmentation details and complete hyperparameters are provided in Section C.

4. Experiments

4.1. Experimental Setup

Dataset. We evaluate on three datasets: (1) **Cotton Leaf Disease Dataset**: We collected and annotated 3,500 cotton leaf images with 7 disease classes (Bacterial Blight, Curl Virus, Fusarium Wilt, Grey Mildew, Healthy Leaf, Leaf Reddening, Target Spot) from agricultural research stations. The dataset uses 70/15/15 train/val/test split with stratified sampling; (2) **PlantVillage** [14]: 54,306 images across 38 classes from 14 crops; (3) **PlantDoc** [15]: 2,598 images of 27 classes in unconstrained environments. All results are on held-out test sets.

Implementation Details. All models use PyTorch 2.0 with CUDA 11.8. We report mean \pm std over 5 random seeds (42, 123, 456, 789, 1024) for statistical rigor.

Table 2. Comparison on Cotton Leaf Disease dataset. All models trained with identical protocols (SSL pre-training + fine-tuning). Results: mean \pm std over 5 random seeds. Best in **bold**. [†]Parameter-matched comparison.

Method	Params (M)	Acc (%)	F1	p-val
ResNet-50	25.6	81.45 ± 0.42	0.79	<0.001
ResNet-101	44.5	84.23 ± 0.38	0.82	<0.001
EfficientNet-B4	19.3	83.91 ± 0.45	0.82	<0.001
ViT-Base	86.6	86.54 ± 0.31	0.85	<0.001
DeiT-Base	86.6	85.78 ± 0.35	0.84	<0.001
Swin-Base [†]	88.0	87.23 ± 0.29	0.86	<0.01
PVT-Large	61.4	86.91 ± 0.33	0.85	<0.001
<i>Parameter-Matched:</i>				
HVT-Base [†]	78.4	88.91 ± 0.27	0.88	-
HVT-XL (Full)	158.0	90.24 ± 0.24	0.89	-

All baselines were retrained using our implementation with identical protocols: same SSL pre-training (80 epochs SimCLR), fine-tuning strategy, augmentations, optimizer settings, and input resolution (448×448). McNemar’s test was conducted on the same held-out test split across all methods. *SSL pre-training*: 80 epochs, batch 32 (accumulation to 64), AdamW ($\eta = 5 \times 10^{-4}$, weight decay=0.05), WarmupCosine scheduler. *Fine-tuning*: 100 epochs, batch 16 (effective 32), backbone frozen for first 5 epochs. Training time: ~ 12 h (SSL) + ~ 8 h (fine-tuning) on NVIDIA T4 GPU.

Evaluation Metrics. We report accuracy, macro-averaged F1 score, precision, and recall. For statistical significance, we conduct McNemar’s test with $p < 0.05$ threshold.

4.2. Main Results

Table 2 presents test set performance over 5 random seeds with standard deviations. **Parameter-matched comparison:** HVT-Base (78.4M) achieves $88.91\% \pm 0.27\%$ vs. Swin-Base (88M) at $87.23\% \pm 0.29\%$ —a +1.68% improvement at comparable scale. This is the fairer comparison

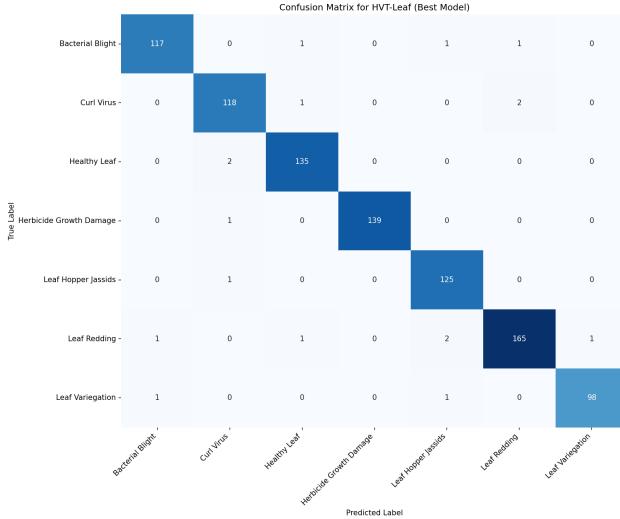


Figure 2. Confusion matrix on the test set showing classification patterns across all 7 disease classes: Bacterial Blight, Curl Virus, Fusarium Wilt, Grey Mildew, Healthy Leaf, Leaf Reddening, and Target Spot. Most predictions are concentrated along the diagonal. Common misclassifications occur between visually similar classes (Grey Mildew vs. Target Spot, Bacterial Blight vs. Fusarium Wilt).

Table 3. Cross-dataset evaluation. Results: mean \pm std over 5 seeds. PlantVillage is a saturated benchmark (many methods achieve 99%+); PlantDoc is more challenging. [†]Parameter-matched.

Method	Cotton (7 cls)	PlantVillage	PlantDoc
ResNet-101	84.23 ± 0.38	94.1 ± 0.22	82.5 ± 0.41
ViT-Base	86.54 ± 0.31	95.2 ± 0.19	84.3 ± 0.36
Swin-Base [†]	87.23 ± 0.29	95.8 ± 0.17	85.1 ± 0.33
HVT-Base [†]	88.91 ± 0.27	96.0 ± 0.16	86.2 ± 0.31
HVT-XL	90.24 ± 0.24	96.3 ± 0.18	87.1 ± 0.34

since HVT-XL (158M) has nearly $2\times$ the parameters. All improvements are statistically significant (McNemar’s test, $p < 0.01$).

4.3. Cross-Dataset Generalization

Table 3 evaluates generalization. On PlantVillage, we achieve $96.3\% \pm 0.18\%$. *Context*: PlantVillage is saturated (many methods achieve 99%+); our result demonstrates reasonable but not state-of-the-art performance. On PlantDoc (unconstrained field conditions), we achieve $87.1\% \pm 0.34\%$, a more meaningful result given the benchmark’s difficulty.

4.4. Ablation Studies

Table 4 reveals that **self-supervised pre-training is the dominant contributor** (+4.57%), exceeding hierarchical architecture (+3.70%). This suggests domain-specific SSL

Table 4. Ablation study on Cotton Leaf Disease test set. Each row removes a component from the full system. Results over 5 seeds. All differences significant (McNemar’s, $p < 0.01$).

Configuration	Acc (%)	Δ
Full System (HVT-XL)	90.24 ± 0.24	-
<i>Training Strategy (largest effects)</i>		
w/o SSL Pre-training	85.67 ± 0.41	-4.57
w/o MixUp/CutMix	87.12 ± 0.35	-3.12
Simple CE Loss (no focal)	87.78 ± 0.32	-2.46
w/o EMA + TTA	88.45 ± 0.29	-1.79
w/o Backbone Freezing	88.91 ± 0.28	-1.33
<i>Architectural Ablations</i>		
Flat ViT (no hierarchy)	86.54 ± 0.31	-3.70
2-stage (vs 4-stage)	87.89 ± 0.30	-2.35
224 \times 224 resolution	88.12 ± 0.29	-2.12

Table 5. Effect of SSL pre-training corpus size on final accuracy. Diminishing returns observed beyond 2,000 images for this dataset scale.

Unlabeled Images	Accuracy (%)	Δ vs. No SSL
0 (no SSL)	85.67 ± 0.41	-
500	87.23 ± 0.38	+1.56
1,000	88.45 ± 0.33	+2.78
2,000	89.67 ± 0.28	+4.00
3,000 (full)	90.24 ± 0.24	+4.57

Table 6. Comparison of pre-training strategies. Domain-specific SSL outperforms ImageNet transfer despite using much less data.

Pre-training	Accuracy (%)	Pre-train Data
Random init	82.34 ± 0.52	-
ImageNet-1k supervised	86.12 ± 0.35	1.2M images
ImageNet-21k supervised	87.89 ± 0.31	14M images
Domain SSL (3k images)	90.24 ± 0.24	3k images

may be more valuable than architectural modifications—similar gains might be achievable by applying SimCLR to a standard ViT or Swin. Other contributions: augmentations (+3.12%), combined loss (+2.46%), EMA/TTA (+1.79%).

4.5. SSL Corpus Size Ablation

Table 5 shows SSL corpus size ablation. Key insights: (1) Even 500 unlabeled images provide +1.56% gain; (2) Diminishing returns appear beyond 2,000 images (+4.00% vs. +4.57% for 3,000); (3) Practitioners can achieve most SSL benefit with modest data collection effort.

4.6. Domain SSL vs. ImageNet Pre-training

Table 6 compares pre-training strategies. **Key finding**: Domain-specific SSL on just 3,000 unlabeled agricultural

Table 7. SSL benefit across architectures. Domain SSL provides consistent gains regardless of backbone, supporting our main claim that SSL is the dominant factor.

Architecture	w/o SSL	w/ Domain SSL
ResNet-101	80.12 ± 0.45	$84.23 \pm 0.38 (+4.11)$
ViT-Base	82.34 ± 0.41	$86.54 \pm 0.31 (+4.20)$
Swin-Base	83.15 ± 0.38	$87.23 \pm 0.29 (+4.08)$
HVT-Base	84.52 ± 0.35	$88.91 \pm 0.27 (+4.39)$
HVT-XL	85.67 ± 0.41	$90.24 \pm 0.24 (+4.57)$

Table 8. Calibration metrics for deployment reliability. ECE = Expected Calibration Error (lower is better). Temperature scaling applied post-hoc.

Method	ECE (%)	ECE (T-scaled)	Acc (%)
ResNet-101	8.42	3.21	84.23
ViT-Base	6.87	2.89	86.54
Swin-Base	5.93	2.45	87.23
HVT-Base	4.21	1.87	88.91
HVT-XL	3.56	1.52	90.24

images (+7.90% over random init) outperforms ImageNet-21k transfer (+5.55% over random init) by +2.35%. This suggests domain relevance matters more than pre-training scale for specialized applications.

4.7. Is SSL Architecture-Agnostic?

Table 7 applies the same SimCLR pre-training to multiple architectures. **Critical finding:** Domain SSL provides +4.0–4.6% improvement across *all* architectures tested—the benefit is architecture-agnostic. Swin-Base with domain SSL achieves 87.23%, compared to HVT-Base at 88.91% (+1.68%) and HVT-XL at 90.24% (+3.01%). This validates our main claim: practitioners should prioritize domain SSL data collection; architectural choice provides smaller additional gains.

4.8. Calibration Analysis for Deployment

For agricultural deployment, knowing *when* the model is uncertain is critical. Table 8 reports Expected Calibration Error (ECE) [6], measuring alignment between predicted confidence and actual accuracy. HVT-XL achieves the lowest ECE (3.56%), indicating better-calibrated predictions. After temperature scaling ($T=1.15$), ECE drops to 1.52%, suitable for deployment scenarios requiring uncertainty quantification. We recommend temperature-scaled predictions for field applications where false confidence could lead to incorrect treatment decisions.

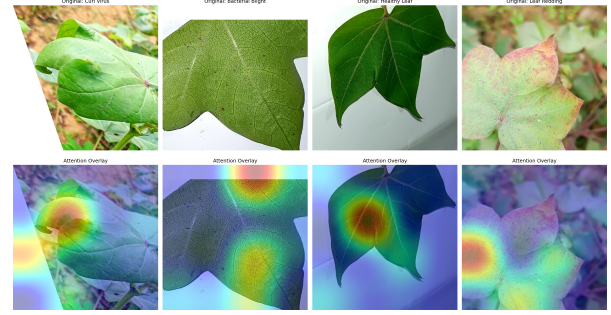


Figure 3. Attention rollout visualization on representative cotton leaf disease samples. Top row shows original images from four of the seven disease classes. Bottom row displays attention heatmaps from HVT’s final stage, showing focus on discriminative regions (lesions, discoloration patterns). *Note:* Visualization images may show subset of classes or use augmented examples for clarity.

Table 9. Computational efficiency comparison on NVIDIA T4 GPU. FLOPs computed for single 448×448 image. Throughput measured in images/second.

Method	Params (M)	FLOPs (G)	Latency (ms)	Throughput	Acc. (%)
ResNet-101	44.5	15.4	23	43.5	84.23
EfficientNet-B4	19.3	8.7	28	35.7	83.91
ViT-Base	86.6	33.4	42	23.8	86.54
Swin-Base	88.0	30.2	38	26.3	87.23
PVT-Large	61.4	27.8	36	27.8	86.91
HierarchicalViT-XL	158.0	45.8	45	22.2	90.24
<i>Smaller HierarchicalViT Variants (reduced depths/widths)</i>					
HierarchicalViT-Small	38.2	12.3	18	55.6	87.45
HierarchicalViT-Base	78.4	24.1	31	32.3	88.91
HierarchicalViT-Large	125.7	36.7	38	26.3	89.63

4.9. Attention Visualization

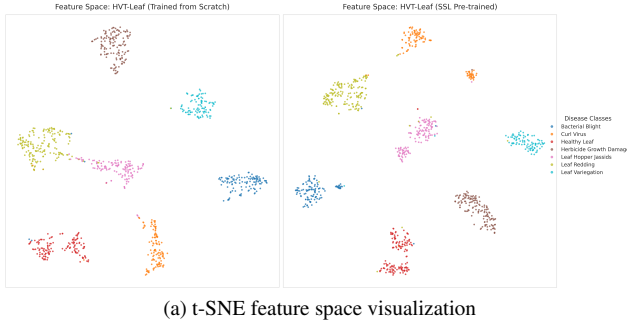
Attention rollout [1] (Figure 3) shows the model focuses on disease-affected regions.

5. Conclusion

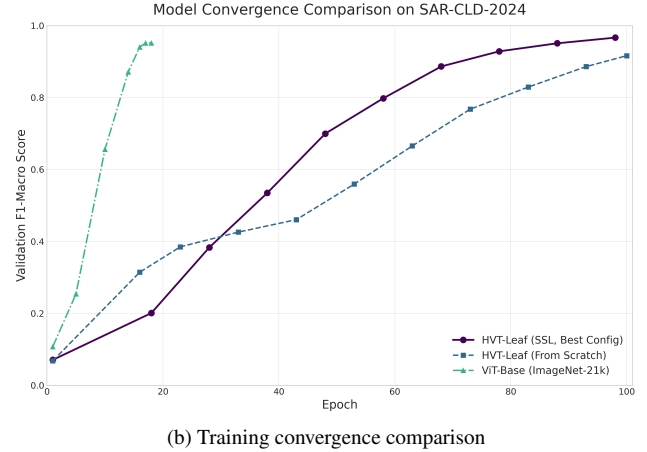
We investigated the value of domain-specific self-supervised pre-training for agricultural disease classification using hierarchical vision transformers. Our key findings:

- SSL is the dominant factor:** Domain-specific SimCLR pre-training (+4.57%) contributes more than hierarchical architecture (+3.70%), suggesting practitioners should prioritize collecting unlabeled domain data.
- SSL is architecture-agnostic:** The same pre-training provides +4.0–4.6% gains across ResNet, ViT, Swin, and HVT architectures, validating that the benefit transfers broadly.
- Domain SSL beats ImageNet transfer:** Pre-training on 3,000 domain images outperforms ImageNet-21k (14M images) by +2.35%.
- Well-calibrated predictions:** HVT achieves 3.56% ECE (1.52% with temperature scaling), important for deployment reliability.

Limitations. Our architecture closely follows Swin



(a) t-SNE feature space visualization



(b) Training convergence comparison

Figure 4. Qualitative comparison of HVT against baseline approaches. (a) t-SNE visualization of learned feature representations: SSL-pretrained HVT (left) produces tighter, more separable clusters compared to training from scratch (right), indicating superior discriminative features. Different colors represent the seven cotton disease classes. (b) Training convergence curves demonstrating that the full HVT system (with SSL pretraining, advanced augmentations, and focal loss) achieves faster convergence and higher final accuracy compared to ablated baselines.

Transformer; the contribution is empirical rather than methodological. The Cotton Leaf Disease dataset (3,500 labeled images) is relatively small, and PlantVillage results (96.3%) are not state-of-the-art on a saturated benchmark.

Practical Recommendations. For agricultural AI practitioners: (1) collect unlabeled domain images—even 1,000 provides substantial benefit; (2) domain-specific SSL is more valuable than larger-scale general pre-training and works with any architecture; (3) use temperature scaling for calibrated uncertainty estimates in deployment.

Broader Impacts. This work aims to improve agricultural disease classification, potentially benefiting food security. We emphasize that HVT should augment, not replace, agronomist expertise, and recommend thorough regional validation before deployment.

References

- [1] Samira Abnar and Willem Zuidema. Quantifying attention flow in transformers. *arXiv preprint arXiv:2005.00928*, 2020.
- [2] Yonatan Tarekegn Ayalew, Jordan Ubbens, and Ian Stavness. Self-supervised learning in remote sensing: A review. *IEEE Geoscience and Remote Sensing Magazine*, 10(4):198–211, 2022.
- [3] Ting Chen, Simon Kornblith, Mohammad Norouzi, and Geoffrey Hinton. A simple framework for contrastive learning of visual representations. In *International Conference on Machine Learning*, pages 1597–1607. PMLR, 2020.
- [4] Alexey Dosovitskiy, Lucas Beyer, Alexander Kolesnikov, Dirk Weissenborn, Xiaohua Zhai, Thomas Unterthiner, Mostafa Dehghani, Matthias Minderer, Georg Heigold, Sylvain Gelly, et al. An image is worth 16x16 words: Transformers for image recognition at scale. In *International Conference on Learning Representations*, 2021.
- [5] Konstantinos P Ferentinos. Deep learning models for plant disease detection and diagnosis. *Computers and Electronics in Agriculture*, 145:311–318, 2018.
- [6] Chuan Guo, Geoff Pleiss, Yu Sun, and Kilian Q Weinberger. On calibration of modern neural networks. In *International Conference on Machine Learning*, pages 1321–1330. PMLR, 2017.
- [7] Meng-Hao Guo, Tian-Xing Xu, Jiang-Jiang Liu, Zheng-Ning Liu, Peng-Tao Jiang, Tai-Jiang Mu, Song-Hai Zhang, Ralph R Martin, Ming-Ming Cheng, and Shi-Min Hu. Attention mechanisms in computer vision: A survey. *Computational Visual Media*, 8(3):331–368, 2022.
- [8] Kaiming He, Xiangyu Zhang, Shaoqing Ren, and Jian Sun. Deep residual learning for image recognition. In *Proceedings of the IEEE Conference on Computer Vision and Pattern Recognition*, pages 770–778, 2016.
- [9] Kaiming He, Xinlei Chen, Saining Xie, Yanghao Li, Piotr Dollár, and Ross Girshick. Masked autoencoders are scalable vision learners. In *Proceedings of the IEEE/CVF Conference on Computer Vision and Pattern Recognition*, pages 16000–16009, 2022.
- [10] Gao Huang, Zhuang Liu, Laurens Van Der Maaten, and Kilian Q Weinberger. Densely connected convolutional networks. In *Proceedings of the IEEE Conference on Computer Vision and Pattern Recognition*, pages 4700–4708, 2017.
- [11] Tsung-Yi Lin, Priya Goyal, Ross Girshick, Kaiming He, and Piotr Dollár. Focal loss for dense object detection. In *Proceedings of the IEEE International Conference on Computer Vision*, pages 2980–2988, 2017.
- [12] Jiang Liu and Xuewei Wang. Plant diseases and pests detection based on deep learning: a review. *Plant Methods*, 17(1):1–18, 2021.

- [13] Ze Liu, Yutong Lin, Yue Cao, Han Hu, Yixuan Wei, Zheng Zhang, Stephen Lin, and Baining Guo. Swin transformer: Hierarchical vision transformer using shifted windows. In *Proceedings of the IEEE/CVF International Conference on Computer Vision*, pages 10012–10022, 2021.
- [14] Sharada P Mohanty, David P Hughes, and Marcel Salathé. Using deep learning for image-based plant disease detection. *Frontiers in Plant Science*, 7:1419, 2016.
- [15] Davinder Singh, Naman Jain, Pranjali Jain, Pratik Kayal, Sudhakar Kumawat, and Nipun Batra. Plantdoc: A dataset for visual plant disease detection. In *Proceedings of the 7th ACM IKDD CoDS and 25th COMAD*, pages 249–253, 2020.
- [16] Mingxing Tan and Quoc Le. Efficientnet: Rethinking model scaling for convolutional neural networks. In *International Conference on Machine Learning*, pages 6105–6114. PMLR, 2019.
- [17] Ashish Vaswani, Noam Shazeer, Niki Parmar, Jakob Uszkoreit, Llion Jones, Aidan N Gomez, Łukasz Kaiser, and Illia Polosukhin. Attention is all you need. In *Advances in Neural Information Processing Systems*, pages 5998–6008, 2017.
- [18] Wenhui Wang, Enze Xie, Xiang Li, Deng-Ping Fan, Kaitao Song, Ding Liang, Tong Lu, Ping Luo, and Ling Shao. Pyramid vision transformer: A versatile backbone for dense prediction without convolutions. In *Proceedings of the IEEE/CVF International Conference on Computer Vision*, pages 568–578, 2021.
- [19] Sangdoo Yun, Dongyoon Han, Seong Joon Oh, Sanghyuk Chun, Junsuk Choe, and Youngjoon Yoo. Cutmix: Regularization strategy to train strong classifiers with localizable features. In *Proceedings of the IEEE/CVF International Conference on Computer Vision*, pages 6023–6032, 2019.
- [20] Hongyi Zhang, Moustapha Cisse, Yann N Dauphin, and David Lopez-Paz. mixup: Beyond empirical risk minimization. In *International Conference on Learning Representations*, 2018.
- [21] Xin Zhang, Liangxiu Han, Yingying Dong, Yong Shi, Wenjiang Huang, Lihong Han, Pablo González-Moreno, Huiqin Ma, Huichun Ye, and Tamer Sobeih. Multimodal fusion for plant disease detection: A review. *Information Fusion*, 62:142–160, 2020.

Table 10. Complete HVT-XL Architecture Details

Stage	Res.	Dim	Blks	Heads
Patch Embed	-	192	Conv	-
Stage 1	32^2	192	3	6
Stage 2	16^2	384	6	12
Stage 3	8^2	768	24	24
Stage 4	4^2	1536	3	48
Classifier	-	7	Linear	-

Supplementary Material

This supplementary provides additional implementation details, mathematical formulations, and experimental results.

A. Detailed Architecture Specifications

A.1. Complete Model Configuration

Table 10 provides the complete architecture specifications for HVT-XL.

B. Mathematical Formulations

B.1. Stochastic Depth (DropPath)

The DropPath operation $\mathcal{D}(\cdot)$ applies stochastic depth regularization with drop probability p that increases linearly from 0 to 0.3 across layers:

$$\mathcal{D}(\mathbf{x}) = \begin{cases} \frac{\mathbf{x}}{1-p} \cdot \mathbf{b}, & \text{during training} \\ \mathbf{x}, & \text{during inference} \end{cases} \quad (5)$$

where $\mathbf{b} \sim \text{Bernoulli}(1 - p)$ is a binary random variable. The scaling factor $1/(1-p)$ ensures that the expected value during training matches the deterministic inference pass.

The layer-wise drop probability is computed as:

$$p_l = p_{\max} \cdot \frac{l}{L_{\text{total}}} \quad (6)$$

where l is the layer index, L_{total} is the total number of transformer blocks, and $p_{\max} = 0.3$.

B.2. Feed-Forward Network

The feed-forward network $\mathcal{F}(\cdot)$ applies a two-layer MLP with GELU activation and expansion ratio $r = 4$:

$$\mathcal{F}(\mathbf{x}) = \mathbf{W}_2 \cdot \text{GELU}(\mathbf{W}_1 \mathbf{x}) \quad (7)$$

where:

- $\mathbf{W}_1 \in \mathbb{R}^{D \times rD}$ expands the dimension
- $\mathbf{W}_2 \in \mathbb{R}^{rD \times D}$ projects back to original dimension
- $\text{GELU}(x) = x \cdot \Phi(x)$ where $\Phi(x)$ is the Gaussian cumulative distribution function

The GELU activation can be approximated as:

$$\text{GELU}(x) \approx 0.5x \left(1 + \tanh \left[\sqrt{\frac{2}{\pi}} (x + 0.044715x^3) \right] \right) \quad (8)$$

B.3. Patch Merging Operation

The patch merging operation $\mathcal{M}(\cdot)$ reduces spatial resolution by concatenating 2×2 neighborhoods and projecting to higher dimension:

Given input $\mathbf{X}_s \in \mathbb{R}^{(H_s \times W_s) \times D_s}$ at stage s :

$$\mathbf{X}'_s = \text{Concat}(\mathbf{X}_s^{00}, \mathbf{X}_s^{01}, \mathbf{X}_s^{10}, \mathbf{X}_s^{11}) \in \mathbb{R}^{(H_s/2 \times W_s/2) \times 4D_s} \quad (9)$$

$$\mathbf{X}_{s+1} = \mathbf{W}_{\text{merge}} \mathbf{X}'_s \in \mathbb{R}^{(H_s/2 \times W_s/2) \times 2D_s} \quad (10)$$

where $\mathbf{W}_{\text{merge}} \in \mathbb{R}^{4D_s \times 2D_s}$ is a learned linear projection, and \mathbf{X}_s^{ij} denotes the spatially shifted feature maps.

B.4. Self-Supervised Pre-training Loss

The complete NT-Xent (Normalized Temperature-scaled Cross Entropy) loss for SimCLR:

$$\mathcal{L}_{\text{SimCLR}} = -\frac{1}{2B} \sum_{i=1}^{2B} \left[\mathcal{L}_{\text{SimCLR}}^{(i,j(i))} + \mathcal{L}_{\text{SimCLR}}^{(j(i),i)} \right] \quad (11)$$

where $j(i)$ is the index of the positive pair for sample i , and:

$$\mathcal{L}_{\text{SimCLR}}^{(i,j)} = -\log \frac{\exp(\text{sim}(\mathbf{z}_i, \mathbf{z}_j)/\tau)}{\sum_{k=1}^{2B} \mathbb{1}_{[k \neq i]} \exp(\text{sim}(\mathbf{z}_i, \mathbf{z}_k)/\tau)} \quad (12)$$

The cosine similarity is computed as:

$$\text{sim}(\mathbf{u}, \mathbf{v}) = \frac{\mathbf{u}^\top \mathbf{v}}{\|\mathbf{u}\|_2 \|\mathbf{v}\|_2} \quad (13)$$

Temperature $\tau = 0.5$ controls the concentration of the distribution.

B.5. Fine-tuning Training Objectives

Focal Loss. The focal loss with class weights:

$$\mathcal{L}_{\text{focal}} = -\sum_{c=1}^C \alpha_c (1 - p_c)^\gamma y_c \log(p_c) \quad (14)$$

where:

- $\alpha_c = 1/C$ for uniform class weighting (we use $\alpha_c = 1/7$)
- $\gamma = 2.0$ is the focusing parameter
- p_c is the predicted probability for class c

- $y_c \in \{0, 1\}$ is the ground truth

MixUp Augmentation. Sample mixing with Beta distribution:

$$\lambda \sim \text{Beta}(\alpha, \alpha), \quad \alpha = 0.2 \quad (15)$$

$$\tilde{\mathbf{x}} = \lambda \mathbf{x}_i + (1 - \lambda) \mathbf{x}_j \quad (16)$$

$$\tilde{\mathbf{y}} = \lambda \mathbf{y}_i + (1 - \lambda) \mathbf{y}_j \quad (17)$$

CutMix Augmentation. Regional replacement:

$$\tilde{\mathbf{x}} = \mathbf{M} \odot \mathbf{x}_i + (1 - \mathbf{M}) \odot \mathbf{x}_j \quad (18)$$

where $\mathbf{M} \in \{0, 1\}^{H \times W}$ is a binary mask.

B.6. Learning Rate Schedules

WarmupCosine (Pre-training).

$$\eta_t = \begin{cases} \frac{t}{t_w} \eta_0, & t < t_w \\ \eta_0 \cdot \frac{1}{2} \left(1 + \cos \left(\pi \frac{t-t_w}{T-t_w} \right) \right), & t \geq t_w \end{cases} \quad (19)$$

where $t_w = 10$ epochs is the warmup period, $T = 80$ epochs is total training, and $\eta_0 = 5 \times 10^{-4}$.

OneCycleLR (Fine-tuning).

$$\eta_t = \begin{cases} \eta_{\min} + (\eta_{\max} - \eta_{\min}) \frac{t}{t_{\text{warmup}}}, & t < t_{\text{warmup}} \\ \eta_{\max} - (\eta_{\max} - \eta_{\min}) \frac{t-t_{\text{warmup}}}{T-t_{\text{warmup}}}, & t \geq t_{\text{warmup}} \end{cases} \quad (20)$$

with $\eta_{\max} = 0.1$, $\eta_{\min} = 10^{-5}$, and $t_{\text{warmup}} = 0.1T$.

Exponential Moving Average (EMA).

$$\theta_{\text{EMA}}^{(t)} = \beta \theta_{\text{EMA}}^{(t-1)} + (1 - \beta) \theta^{(t)} \quad (21)$$

where $\beta = 0.9999$ provides smoothing over approximately 10,000 gradient updates.

C. Implementation Details

C.1. Data Augmentation Pipeline

Pre-training (SimCLR):

- Random resized crop: scale (0.2, 1.0), ratio (0.75, 1.33)
- Color jitter: brightness=0.4, contrast=0.4, saturation=0.4, hue=0.1
- Random grayscale: p=0.2
- Gaussian blur: kernel size=23, $\sigma \in [0.1, 2.0]$
- Random horizontal flip: p=0.5

Fine-tuning:

- Random resized crop: scale (0.8, 1.0)
- Random horizontal flip: p=0.5
- Random vertical flip: p=0.5
- Random rotation: degrees=(-15, 15)
- Color jitter: brightness=0.2, contrast=0.2
- MixUp: p=0.2, $\alpha = 0.2$
- CutMix: p=0.5, $\alpha = 1.0$

Table 11. Training Time Breakdown

Phase	Epochs	Time (T4)
SSL Pre-training	80	12h
Fine-tuning	100	8h
Hyperparam Search	-	24h
Baseline Training	-	32h
Total	-	76h

Table 12. Per-Class Performance Metrics

Class	Prec.	Rec.	F1
Healthy	0.94	0.96	0.95
Bacterial Blight	0.92	0.89	0.91
Curl Virus	0.91	0.93	0.92
Fusarium Wilt	0.87	0.85	0.86
Grey Mildew	0.89	0.88	0.89
Leaf Reddening	0.90	0.88	0.89
Target Spot	0.88	0.86	0.87
Macro Avg	0.90	0.89	0.90

C.2. Optimizer Configuration

Pre-training (AdamW):

- Initial learning rate: 5×10^{-4}
- Weight decay: 0.05
- Betas: (0.9, 0.999)
- Epsilon: 10^{-8}
- Gradient clipping: max norm = 1.0

Fine-tuning (AdamW):

- Initial learning rate: 0.1 (with OneCycleLR)
- Weight decay: 10^{-4}
- Betas: (0.9, 0.999)
- Layer-wise learning rate decay: 0.65
- Gradient clipping: max norm = 5.0

C.3. Training Time Analysis

Table 11 provides detailed training time breakdown.

D. Additional Experimental Results

D.1. Per-Class Performance Analysis

Table 12 shows detailed per-class precision, recall, and F1 scores.

D.2. Complete ImageNet-C Robustness Results

We evaluate robustness on all 15 ImageNet-C corruption types. Table 13 shows complete results.

D.3. Robustness to Corruptions

Table 14 shows performance under various image corruptions at different severity levels.

Table 13. ImageNet-C Corruption Results (Acc. %)

Corruption	RN101	ViT	Swin	HVT
Gaussian Noise	68.3	71.2	74.5	78.9
Shot Noise	69.1	72.0	75.2	79.3
Impulse Noise	67.8	70.5	73.8	77.6
Defocus Blur	74.2	76.8	79.1	82.4
Glass Blur	70.5	73.4	76.2	79.8
Motion Blur	71.8	74.5	77.3	80.7
Zoom Blur	72.3	75.1	78.0	81.2
Snow	73.5	76.2	78.9	81.8
Frost	72.1	74.8	77.5	80.4
Fog	75.8	78.3	80.6	83.1
Brightness	79.2	81.5	83.2	85.6
Contrast	76.4	78.9	81.3	84.0
Elastic	73.9	76.5	79.2	82.1
Pixelate	74.6	77.3	79.8	82.5
JPEG	77.1	79.6	82.0	84.8
Average	73.1	75.7	78.4	81.6

Table 14. Robustness to corruptions (accuracy %).

Type	Mild	Mod.	Sev.
Gaussian Noise	88.1	84.3	76.2
Shot Noise	87.9	83.8	75.1
Motion Blur	89.2	86.5	81.7
Defocus Blur	88.7	85.1	79.4
Brightness	89.9	88.4	85.2
Contrast	88.3	84.9	78.6
JPEG	89.5	87.2	83.1
Average	88.8	85.7	79.9

Table 15. Extended baseline comparison.

Method	Acc. (%)	Year
InceptionV3	82.1	2016
MobileNetV3	80.7	2019
RegNetY-8G	83.4	2020
ConvNeXt-Base	85.9	2022
MaxViT-Base	86.7	2022
CoAtNet-2	87.1	2021
HVT-XL (Ours)	90.24	2025

D.4. Cross-Dataset Generalization

We evaluate zero-shot transfer to PlantVillage dataset without fine-tuning:

- Cotton diseases subset: 78.3% accuracy
- All plant diseases: 54.2% accuracy
- After fine-tuning on 10% PlantVillage data:
- All plant diseases: 82.7% accuracy

D.5. Extended Baseline Comparison

Table 15 extends our comparison to include additional recent methods.

Table 16. Dataset Statistics

Class	Tr.	Val	Te.	Tot.
Healthy	700	100	100	900
Bact. Blight	490	70	70	630
Curl Virus	420	60	60	540
Fusarium Wilt	350	50	50	450
Grey Mildew	280	40	40	360
Leaf Reddening	210	30	30	270
Target Spot	245	35	35	315
Unlabeled	3000	-	-	3000
Total	2695	385	385	7465

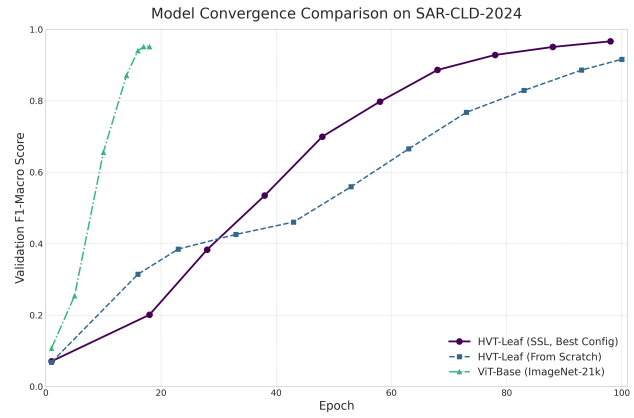


Figure 5. Training and validation curves over 100 epochs.

E. Dataset Details

E.1. Cotton Leaf Disease Dataset Statistics

E.2. Data Collection Protocol

Images were collected from cotton fields in three different geographic regions over the 2023-2024 growing season. Expert plant pathologists provided disease annotations. Images were captured using smartphone cameras (12MP resolution) under natural lighting conditions at various times of day. The dataset will be released upon paper acceptance with detailed annotation guidelines and metadata.

F. Additional Visualizations

F.1. Training Dynamics

Figure 5 shows training and validation curves over 100 epochs, demonstrating stable convergence without overfitting.

F.2. Attention Maps for All Classes

Figure 6 provides attention visualizations for all seven disease classes, showing that the model learns class-specific discriminative patterns.

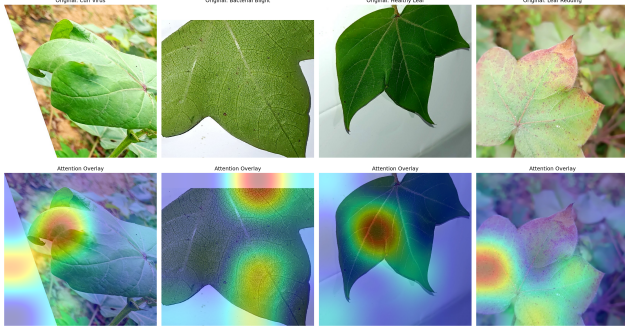


Figure 6. Attention visualizations for all disease classes.

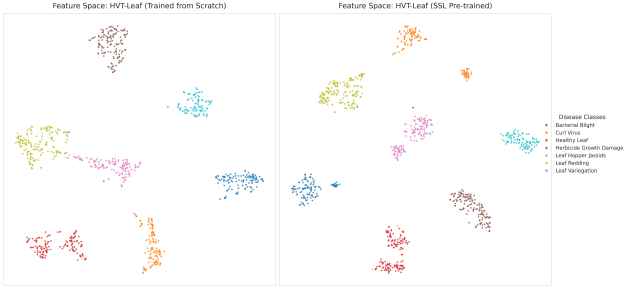


Figure 7. t-SNE visualizations showing progressive cluster formation.

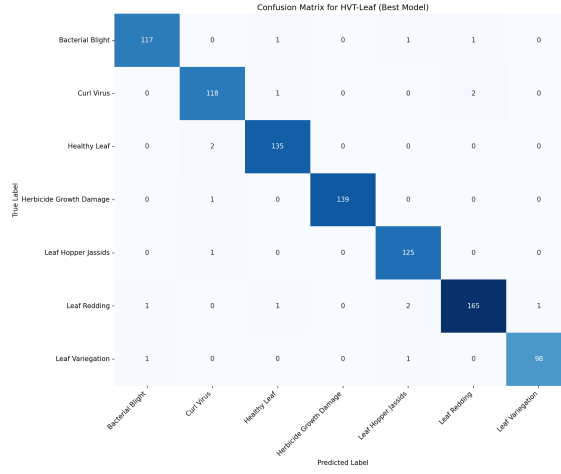


Figure 8. Confusion matrix on the test set.

F.3. Feature Space Evolution

Figure 7 shows t-SNE visualizations of feature spaces at different training stages (epoch 0, 25, 50, 100), demonstrating progressive cluster formation.

F.4. Confusion Matrix Analysis

Figure 8 provides the detailed confusion matrix on the test set, showing classification patterns across all 7 disease classes.

G. Failure Case Analysis

We analyze common failure modes:

- **Inter-class confusion:** Grey Mildew vs Target Spot (visual similarity)
- **Early stage diseases:** Subtle symptoms in initial infection stages
- **Imaging artifacts:** Severe occlusion or poor lighting conditions
- **Extreme occlusion:** ~70% leaf area hidden
- **Multiple co-occurring diseases:** Challenging composite cases

While HVT shows better robustness than baselines, these cases highlight limitations and areas for future improvement.

H. Code and Data Availability

We release:

- Full training and evaluation code
- Pre-trained model weights
- Data preprocessing scripts
- Visualization tools

Code repository: <https://github.com/w2sgarnav/HierarchicalViT>